Journal of Holography Applications in Physics
Volume 4, Issue 3, Summer 2024, 19–34
©Available online at http://jhap.du.ac.ir
DOI: 10.22128/jhap.2024.843.1087
Online ISSN: 2783–3518

Regular article

Chiral Symmetry Breaking and the Critical Point in QCD-like Theories

Kazem Bitaghsir Fadafan[1] · Mansoureh Gholamzadeh[2]

[1] Faculty of Physics, Shahrood University of Technology, P.O.Box 36199–95161 Shahrood, Iran;
Corresponding Author E-mail: bitaghsir@shahroodut.ac.ir

[2] Faculty of Physics, Shahrood University of Technology, P.O.Box 36199–95161 Shahrood, Iran;
E-mail: mgh.gholamzadeh@gmail.com

Received: June 21, 2024; **Revised:** September 7, 2024; **Accepted:** September 15, 2024

Abstract. This study employs holography within a modified D3/D7 framework to explore the phase diagram of a QCD-like theory. The corresponding dual theory is characterized by a large N, $\mathcal{N} = 4$ gauge theory, integrated with quenched $\mathcal{N} = 2$ quark matter and a novel dilaton profile. The research focuses on how the critical point's location in the phase diagram is influenced by temperature and chemical potential. Additionally, the study examines the trajectory of these critical points in response to alterations in the dilaton profile's control parameter, revealing a trend where the critical endpoint shifts to higher temperatures and lower chemical potentials.

Keywords: Holography; D3/D7 Branes; Chiral Symmetry Breaking; Critical Point.

1 Introduction

The phase diagram of Quantum Chromodynamics (QCD) is a fundamental aspect of understanding the behavior of strong interactions under various conditions [1]. The transition from a confining phase with chiral symmetry breaking to a deconfined phase without chiral symmetry breaking is a key feature of this diagram. In the case of QCD with massless quarks, the phase transition is expected to be first order at low temperatures and high densities. This means that the transition between the phases is abrupt and involves a latent. As the density decreases and the temperature increases, the transition becomes second order, characterized by a continuous change and no latent. At finite quark masses, the second order transition is replaced by a crossover, where the change between phases is smooth and does not involve a phase transition in the strict sense. The critical point, or tri-critical point in some descriptions, is where the line of first order phase transitions ends and the crossover begins. This point is of particular interest because it is the end point of the first order phase transitions line in the QCD phase diagram [3]. The search for and study of the critical point is an active area of research, as it has implications for understanding the early universe, the interior of neutron stars, and the results of heavy ion collision experiments [2]. The exact location and nature of the critical point are still subjects of theoretical investigation and experimental searches. Lattice QCD is helpful to study the phase diagram [4].

In this paper, we study how the chiral symmetry breaking affects the critical point in the QCD-like theories. They refer to theories that share some properties with QCD but may differ in certain aspects, such as the number of colors, flavors, or the presence of additional symmetries. These theories are useful in exploring different regimes of the strong interaction and in understanding phenomena that are difficult to study directly in QCD due to its computational complexity, especially in the non-perturbative regime [3]. For example, the study of QCD at high temperatures and densities is relevant for understanding the early universe and the interior of neutron stars. In these extreme conditions, hadronic matter is expected to undergo a phase transition to a quark-gluon plasma (QGP), where quarks and gluons are no longer confined within hadrons. The phase diagram of QCD-like theories helps researchers explore this transition and the properties of the QGP [5,6].

We use the AdS/CFT correspondence or holography [7–9] to study the phase diagram. The exploration of phase diagrams in gauge theories through holographic methods is a fascinating area of research, especially when it involves features similar to those found in QCD. We consider the D3/D7 setup to introduce quarks in the theory [10–12]. This geometry plays a significant role in the exploration of gauge/gravity duality [13]. It involves D3-branes, which are objects in string theory where open strings can end, and D7-branes, which extend in additional dimensions. The D3-branes are typically associated with a four-dimensional $\mathcal{N}$=4 supersymmetric Yang-Mills theory (SYM), while the D7-branes introduce flavors in the form of fundamental matter, enriching the gauge theory with $\mathcal{N}$=2 supersymmetry when intersecting with the D3-branes. In this configuration, the D7-branes are embedded in the ten-dimensional space that the D3-branes inhabit, intersecting them in such a way that additional symmetries and fields are introduced into the gauge theory. This allows for the study of phenomena such as chiral symmetry breaking and meson spectra in a strongly coupled regime, analogous to QCD [14]. The D3/D7 setup has been instrumental in modeling some aspects of beyond standard model of particle physics [15] and has provided insights into the behavior of strongly coupled systems in neutron stars [16].

It is important to notice that in the basic D3/D7 framework, the depiction of the massive quark phase that is deconfined and exhibits chiral symmetry breaking is somewhat crude. This is primarily because the quark mass is introduced manually as a fixed parameter. Given that the gauge coupling in $\mathcal{N} = 4$ SYM is conformal, one might not expect the IR action to

mirror the increase in the gauge coupling strength. However, it is relatively straightforward to devise a model inspired by D3/D7 that incorporates a mechanism for explicit chiral symmetry breaking. Such a model would accurately capture the essence of a deconfined yet massive quark phase. We intend to explore this avenue and examine how it influences the phase diagram of a theory that resembles QCD. This exploration could provide deeper insights into the non-perturbative aspects of gauge theories and the dynamics of chiral symmetry breaking. For example, in [17] the simple holographic D3/D7 system models a massive, deconfined quark phase in QCD. But the study of [16] revises the equation of state to be stiffer, accommodating exotic dense stars, by introducing a running anomalous dimension for the quark condensate, leading to dynamic chiral symmetry breaking and a non-monotonic speed of sound.

The introduction of a new dilaton profile to control the anomalous condensate of quark-antiquark pairs is an innovative approach. It is intriguing to see how this dilaton profile affects the chiral symmetry breaking, which is a pivotal phenomenon in understanding the behavior of strong interactions. The parameter q that was introduced in [18] to describe chiral symmetry breaking seems to play a significant role in determining the location of the tri-critical point in the phase diagram. This could potentially lead to new insights into how variations in these fundamental parameters can affect the properties of the theory. By varying the parameter q, the behavior of the massive and massless scalar quasinormal modes has been studied in [19]. This paper contributes to the ongoing efforts to understand the complex landscape of gauge theories and their phase transitions, which have implications for both theoretical studies and experimental searches in high-energy physics. The dependence of the critical point on the chiral symmetry breaking parameter q is particularly compelling aspect that could offer new perspectives on the nature of these theories. Using machine learning, the flavor dependent critical point has been studied in [28] from holography. It was shown in [29] that the critical phenomena at the tri critical point in the D3/D7 geometry are very well described by the mean field theory and conventional Landau theory. That would be interesting to investigate the critical phenomena in the presence of q parameter and in the QCD-like theories. Also studying critical phenomena in non equilibrium steady states with an electric field [30] would be interesting in this adapted D3/D7 background.

The paper is organized as follows: Section 2 reviews the adapted D3/D7 spacetime. Section 3 computes thermodynamic quantities. Section 4 presents the effect of the dilaton profile on D7 brane embeddings. The main results and conclusions are summarized in Section 5.

2 The adapted bottom-up D3/D7 geometry

In this section, we review the simple D3/D7 model in the presence of the dilaton profile [14,18] The $\mathcal{N} = 4$ gauge theory at finite temperature has a holographic description in terms of an AdS_5 black hole geometry (with N D3 branes at its core). The geometry is

$$ds^2 = \frac{r^2}{R^2}(-f(r)dt^2 + d\vec{x}^2) + \frac{R^2}{r^2 f(r)}dr^2 + R^2 d\Omega_5^2, \tag{1}$$

where $R^4 = 4\pi g_s N \alpha'^2$ and

$$f(r) = 1 - \frac{r_H^4}{r^4}, \qquad r_H = \pi R^2 T. \tag{2}$$

Here r_H is the position of the black hole horizon which is related to the temperature T of the theory.
It is useful to make the coordinate transformation so that

$$\frac{dr^2}{r^2 f} \equiv \frac{dw^2}{w^2},$$

then one finds

$$w = \sqrt{r^2 + \sqrt{r^4 - r_H^4}}, \tag{3}$$

with $w_H = r_H$. In the new coordinates, a flat 6-plane is perpendicular to the horizon. We will then write the coordinates in that plane as new coordinates ρ and L as

$$\begin{aligned} w &= \sqrt{\rho^2 + L(\rho)^2}, \\ \rho &= w \sin\theta, \\ L(\rho) &= w \cos\theta, \end{aligned} \tag{4}$$

The metric is then

$$ds^2 = \frac{w^2}{R^2}(-g_t dt^2 + g_x d\vec{x}^2) + \frac{R^2}{w^2}(d\rho^2 + \rho^2 d\Omega_3^2 + dL^2 + L^2 d\Omega_1^2) \ , \tag{5}$$

where g_t and g_x are given by

$$g_t = \frac{(w^4 - w_H^4)^2}{2w^4(w^4 + w_H^4)},$$

$$g_x = \frac{w^4 + w_H^4}{2w^4}.$$

In the quench limit $N_f \ll N_c$, $\mathcal{N} = 2$ quark superfields can be included in the $\mathcal{N} = 4$ gauge theory through introducing the probe D7 branes in the background. From holography, one may consider the D3-D7 open strings as the quarks or flavors and the D7-D7 open strings as mesonic operators and their sources. The D7 brane probe can be described by the DBI action as

$$S_{DBI} = -T_{D7} \int d^8\xi h(w) \sqrt{-\det(P[G]_{ab} + 2\pi\alpha' F_{ab})}, \tag{6}$$

where $P[G]_{ab}$ is the pullback of the background metric. Comparing with [14], a new ingredient function $h(w)$ triggers chiral symmetry breaking in the system by introducing parameter q. This parameter is related to the anomalous dimension in the system. It is given by

$$h(w) = 1 + \frac{1}{w^q}. \tag{7}$$

We embed the D7 branes in the ρ and Ω_3 directions of the background metric but to allow all possible D7 brane embeddings must include at constant Ω_1 a profile $L(\rho)$. The function h, which plays a pivotal role in our model, acts as an effective dilaton field. In top-down constructions, the dilaton typically remains constant for $\mathcal{N} = 4$ SYM theory, or in more intricate scenarios, it might influence the spacetime geometry. However, adopting a bottom-up perspective, we permit h to exhibit significant behavior without considering its impact on the metric. It is instrumental in instigating chiral symmetry breaking. A concrete example

of such a mechanism, where a non-trivial dilaton field does not alter the metric yet leads to symmetry breaking, is seen in the case of magnetic field B induced chiral symmetry breaking, as detailed in [20]. In our approach, we will confine our attention to dilaton functions h that asymptotically approach a constant value in the UV regime. This constraint ensures that our model remains consistent with the expected UV behavior of gauge theories.

One should notice that in holographic QCD models, the dilaton is often mapped to the running anomalous dimension of the $q\bar{q}$ operator. This mapping is crucial because it's related to the dynamics of chiral symmetry breaking. Chiral symmetry breaking occurs when the running of the anomalous dimension reaches a point where the chirally symmetric state where the flat D7 brane embedding $L(\rho) = 0$ becomes unstable. This instability leads to the formation of a chiral condensate, signaling the breaking of chiral symmetry. From AdS/CFT correspondence, the chiral condensate is represented by a scalar field in AdS space, and the gauge dynamics are input through the radial dependence of its mass, which represents the running of the anomalous dimension of the $q\bar{q}$ operator. The running anomalous dimension leads to chiral symmetry breaking when it reaches a critical value, and this can be modeled holographically. These insights are significant for understanding the non-perturbative aspects of QCD and have implications for the study of technicolor theories and the search for a light techni-dilaton, which could be a lighter composite scalar in models beyond the Standard Model [15]. It is crucial to underscore that this analysis, to a certain extent, justifies the decision to overlook the backreaction of the dilaton factor within our framework. Should one opt for a fully backreacted geometry, the resultant action's expansion for perturbations around the flat embedding would undoubtedly become more intricate. However, the supplementary components derived from the expansion of metric terms would merely contribute to the running mass of the scalar field in the AdS space. When examining the precursors to chiral symmetry breaking, the introduction of a specifically chosen dilaton can be equally effective as the incorporation of a more complex, bottom-up geometric construction. Nevertheless, a comprehensive and accurate depiction of a specific chiral symmetry breaking scenario would necessitate a careful consideration of these nuances. We continue the derivations by finding the lagrangian from the DBI action as

$$\begin{aligned}\mathcal{L} &= -N_f T_{D7}\frac{\rho^3}{4}\left(1-(\frac{w_H^4}{w^4})^2\right)h(w) \\ &\quad\times\sqrt{\left(1+(\partial_\rho L)^2-\frac{2w^4(w^4+w_H^4)}{(w^4-w_H^4)^2}(2\pi\alpha'\partial_\rho A_t)^2\right)}.\end{aligned} \tag{8}$$

There are two main D7 brane embeddings in the background. The black hole embedding is the one that touches the black hole horizon and the Minkowski one that ends outside of the black hole horizon. The equation of motion of these solutions is solved numerically from the horizon or origin for black hole and Minkowski embeddings, respectively. The embeddings become flat at large distances close to the boundary taking the form

$$L(\rho) \sim m + \frac{c}{\rho^2}. \tag{9}$$

By fitting the D7 brane embeddings with (9) at large ρ, one reads of the quark mass and the condensation.

3 Thermodynamic quantities

In this section, we find the thermodynamics quantities in the system. Since the action (8) is independent of A_t, there is a conserved quantity

$$d = \frac{\delta S}{\delta F_{\rho t}},$$

and we can use the Legendre transformed action

$$\mathcal{L} \to \mathcal{L} - (\partial_\rho A_t)\frac{\delta \mathcal{L}}{\delta(\partial_\rho A_t)}.$$

From the equation of motion one finds that d is a conserved quantity and

$$\partial_\rho A_t = \ d\ \frac{(\omega^4-\omega_H^4)^2}{\omega^4(\omega^4+\omega_H^4)}\sqrt{\frac{4(1+(\ L')^2)}{8\ d^2(\frac{(\omega^4-\omega_H^4)^2}{\omega^4(\omega^4+\omega_H^4)})+h^2\rho^6(1-\frac{\omega_H^8}{\omega^8})^2}}. \tag{10}$$

Now, regarding the values of d one finds

- A trivial solution of (10) with $d = 0$ and constant A_t means that the D7 brane embeddings are those with zero chemical potential.
- When d is non zero, one finds from (10) that A_t' is singular at the origin $\rho = 0$ and requires a charge source so that the electric displacement ends on that source.

One should notice that the charge source is the end point of open strings stretching between the D7 brane embeddings and the black hole horizon. In the case of the D7 brane black hole embeddings, the open string tension pulls them to the black hole horizon. For such a D7 black hole embedding the chemical potential (μ) is defined from the AdS/CFT dictionary as

$$\mu = \int_{\rho_H}^{\infty} d\rho\ d\ \frac{(\omega^4-\omega_H^4)^2}{\omega^4(\omega^4+\omega_H^4)}\sqrt{\frac{4(1+(\ L')^2)}{8\ d^2(\frac{(\omega^4-\omega_H^4)^2}{\omega^4(\omega^4+\omega_H^4)})+h^2\rho^6(1-\frac{\omega_H^8}{\omega^8})^2}}, \tag{11}$$

where one should fix $A_t(\rho_H) = 0$ for a well defined A_t at the black hole horizon.
In the context of the AdS/CFT correspondence, the Euclidean bulk on-shell action plays a crucial role in obtaining the thermodynamic potential of the boundary theory. The grand potential Ω and the Helmholtz free energy F are associated with the action (8) and its Legendre transformation, receptively. The Helmholtz free energy is related to the grand potential through a Legendre transformation, which typically involves the exchange of variables between conjugate pairs, such as entropy and temperature or volume and pressure. It is important to note that these thermodynamic potentials are used to describe different ensembles in statistical mechanics: the grand potential is used in the grand canonical ensemble, where the system can exchange both energy and particles with the environment, while the Helmholtz free energy is used in the canonical ensemble, where the system can exchange energy but not particles.

4 Effect of q parameter on the thermal phase transitions

To clarify the interpretation of the figures that will be discussed in this paper, let's take Figure 1 as an illustration. It consists of three distinct rows:

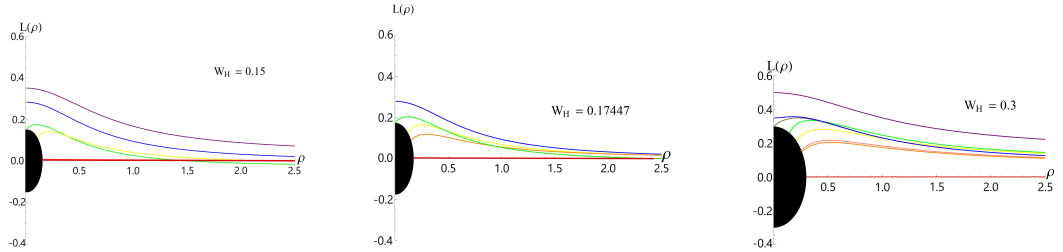

(a) The D7 brane embeddings

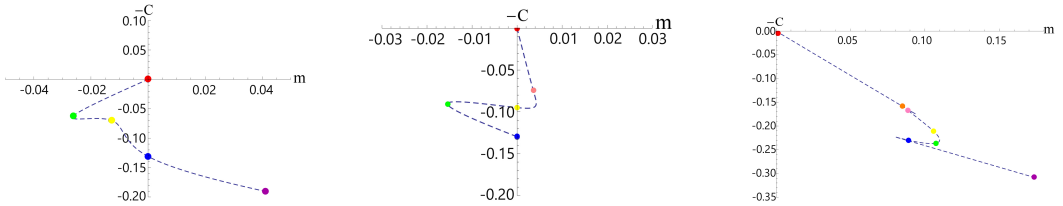

(b) The condensation as a function of quark mass

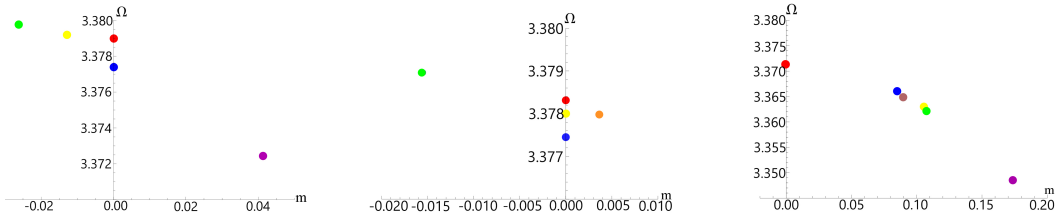

(c) Free energies

Figure 1: Effect of finite temperature on the D7 brane embeddings (first row), the corresponding $c-m$ values (second row) and free energies (third row) at fixed chiral symmetry breaking parameter $q = 1.6$ and zero density.

- The first row presents the D7 brane embedding configurations.
- The second row depicts a graph representing the permissible range for the condensate's value, plotted against the quark mass.
- The third row illustrates the associated thermodynamic potential.

Each of these rows corresponds to a specific value of parameter q that is being held constant throughout. This systematic arrangement allows for a comprehensive analysis of the effects of parameters on the various physical quantities and configurations being studied. Every point in the middle and third plots correspond to one embedding curve in the first row plots. These dot points are color coded with the colors common across each of the figures in the paper.

It is important to notice that the middle diagrams allow for the identification of the first order phase transition points through the application of a Maxwell construction (the equal area law). This technique is corroborated by the presence of a minimum in the grand potential, as depicted on the third row plots. The crossing with the vertical axis line that appear in both the middle and third diagrams denote the location of the phase transition within the system.

First we consider $d = 0$ and fix $q = 1.6$. In the first row of Figure 1, we present results for the $D7$ brane embeddings. From left to right temperature is increasing from $w_H = 0.15$ to $w_H = 0.3$. Correspondingly, one finds that the radius of the black bulb at the origin is increasing. This bulb represents the black hole. Two types of the embeddings are clear from this figure, the Minkowski D7 brane embedding starts at $\rho = 0$ but the black hole D7 brane embeddings start from the black hole horizon.

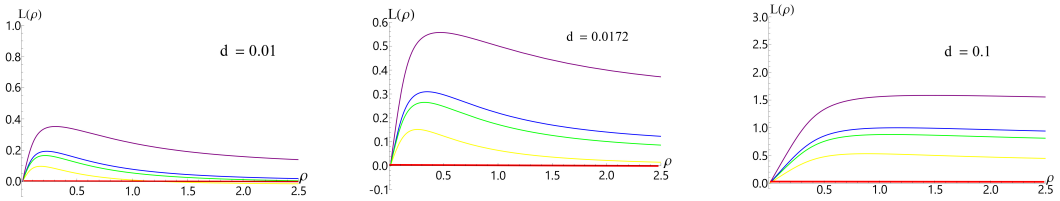

(a) The D7 brane embeddings

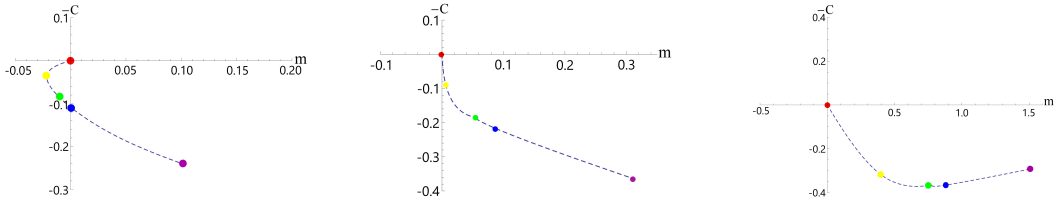

(b) The condensation as a function of quark mass

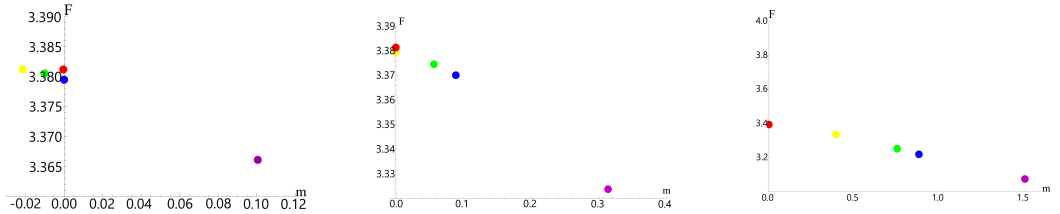

(c) Free energies

Figure 2: Effect of finite density on the D7 brane embeddings (first row), the corresponding $c-m$ values (second row) and free energies (third row) at fixed chiral symmetry breaking parameter $q = 1.6$ and zero temperature.

As mentioned, each point displayed on the second and third rows are associated with a single curve depicted on the first row of the figure. Using (9), we show condensation c as a function of the quark mass m in the second row of Figure 1. Among the D7 brane embeddings, there is only one in which the quark mass goes to zero at UV. It looks a flat embedding at the bottom of the black hole D7 brane embeddings (red color) in the first row of Figure 1. It is shown by a red dot at the origin of $c - m$ plot. One finds that at UV or large ρ the stable solution with zero quark mass $m = 0$ has a non zero condensation c which means chiral symmetry is broken. In the $L - \rho$, the $U(1)$ symmetry is also broken by these embeddings. There should be a first order phase transition between Minkowski and black hole embeddings. But as one finds when we increase the temperature, this transition point disappears in the system.

In the third row, we plotted the corresponding free energies. As one finds the value of the free energy for Minkowski solutions is smaller than the black hole solutions and the reason is the Minkowski solutions are more stable and that's why their free energy is lower.

From Figure 1, we conclude that by increasing the temperature the radius of the black hole horizon grows and the zero quark mass ($m = 0$) D7 brane embeddings become disfavored. Then the first order phase transition occurs in the system and mesons melt, see [23–27]. However, as it was discussed in [12] the spectrum of mesons is stable for Minkowski D7 brane embeddings but the quasi normal modes of the D7 brane black hole embeddings show an imaginary part to the meson spectrum [21,22].

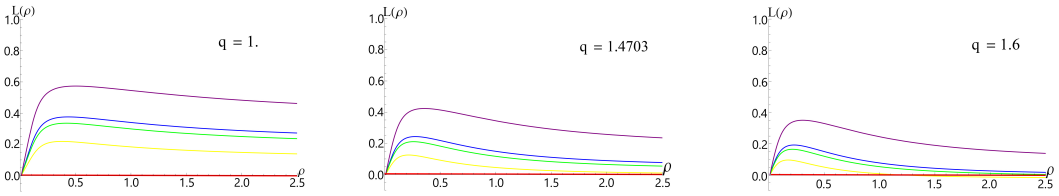

(a) The D7 brane embeddings

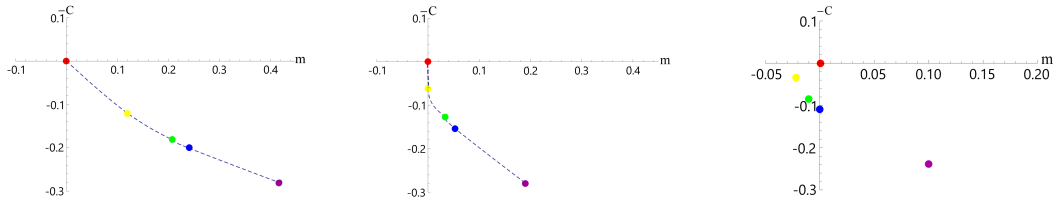

(b) The condensation as a function of quark mass

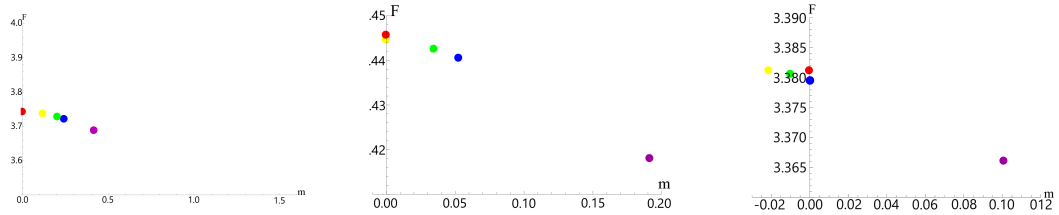

(c) Free energies

Figure 3: Effect of chiral symmetry breaking parameter q on the D7 brane embeddings (first row), the corresponding $c - m$ values (second row) and free energies (third row) at zero temperature and finite density $d = 0.01$.

At zero temperature, we consider finite d or μ in the system at fixed $q = 1.6$ in Figure 2. Such system at $q = 0$ has been studied in [31] and analytic solutions for both black hole and Minkowski D7 brane embeddings have been found. It is difficult to find analytic solutions at finite q and we solve the equations of motion numerically. As one finds from the first row of Figure 2, D7 brane embeddings deform at finite density although there is no a black hole at the center of the geometry. It is clearly seen that a spike is forming at the origin. In the boundary field theory, the interpretation is forming of quarks in the vacuum. One finds that the density is increasing from left to right.

From the second row of Figure 2, a spiral structure is forming at small density but at high d it is difficult to observe it because of numeric issues. Perhaps it disappears at high finite density in the system. A second order chiral symmetry breaking occurs in the system as well. We will further check how it will be affected by q parameter in the system. By increasing the density, the condensation value falls to more negative values.

In examining the Figure 2, we observe that at low densities, there are two distinct

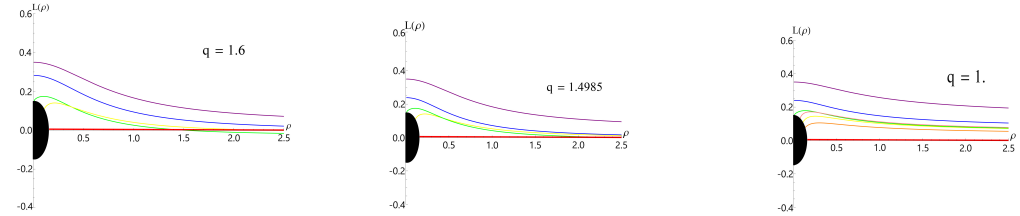

(a) The D7 brane embeddings

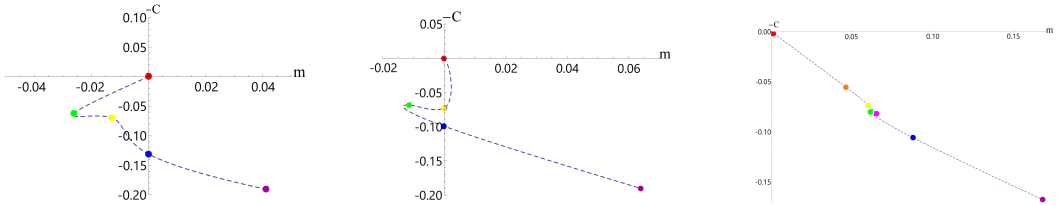

(b) The condensation as a function of quark mass

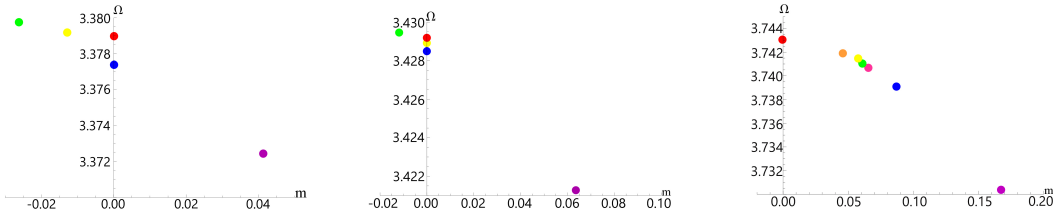

(c) Free energies

Figure 4: Effect of chiral symmetry breaking parameter q on the D7 brane embeddings (first row), the corresponding $c - m$ values (second row) and free energies (third row) at finite temperature.

solutions where the quark mass approaches zero in the UV regime, represented by the blue and red lines. Specifically, at a density value of $d = 0.01$, both solutions exhibit a quark mass of zero, as seen in the first and second rows. To determine the more energetically favorable solution, we turn our attention to the third row. Here, the solution represented by the blue line is associated with lower energy, indicating it is the energetically preferred state in this scenario. This lower energy state suggests that it is the more stable of the two under the given conditions, aligning with the principle that systems tend to the state of minimum energy thermodynamically.

A key insight from Figure 2 is the identification of a critical density, denoted as d_c, at which the condensate value drops to zero. This is clearly depicted in the central graph of the second row. Such a phenomenon suggests the occurrence of a second-order phase transition, leading to a novel phase characterized by the absence of a chiral condensate. The embeddings of the D7 brane for densities below or above d_c are illustrated in the top row, providing a visual representation of the system's behavior across the critical threshold.

Exploring the dynamics of the D7 brane embeddings, condensate-mass, and free energies as a function of the parameter q indeed presents an intriguing line of inquiry. By plotting figures analogous to Figures 1 and 2 , with q as the variable while maintaining a constant density, one can observe the system's response to changes in q. The pivotal finding in Figures 3 and 4 is the critical point q_c, where the system transitions through a second-

order phase change. This can be seen easily from the second row of Figure 3. This critical point marks a significant shift in the system's properties, akin to the critical density d_c previously discussed, but here it is the chiral symmetry breaking parameter q that is the focus. Investigating the underlying reasons for the existence of such a critical value q_c could shed light on the mechanisms of chiral symmetry breaking in the system. It would be particularly interesting to examine how the D7 brane's configuration alters as q approaches q_c, and what implications this has for the phase structure of the theory. Such an analysis could provide deeper insights into the nature of the phase transitions occurring in the model and the physical significance of the parameter q. Also the spiral appears at larger $q > q_c$.

5 Summary and discussions

To create the phase diagram, we have taken cross-sections at constant temperatures while altering the chemical potential. This method allows us to observe how the system's behavior changes across different chemical potentials at a specific temperature, which is crucial for understanding the phase transitions and critical points within the diagram. By systematically varying the chemical potential and documenting the resulting phases, we can map out the regions of chiral symmetry breaking, meson stability, and the conditions under which mesons melt into their constituent quarks. This comprehensive mapping forms the basis of the phase diagram, illustrating the different states of matter under various temperature and density conditions in the massless theory. Studying phase diagrams within different

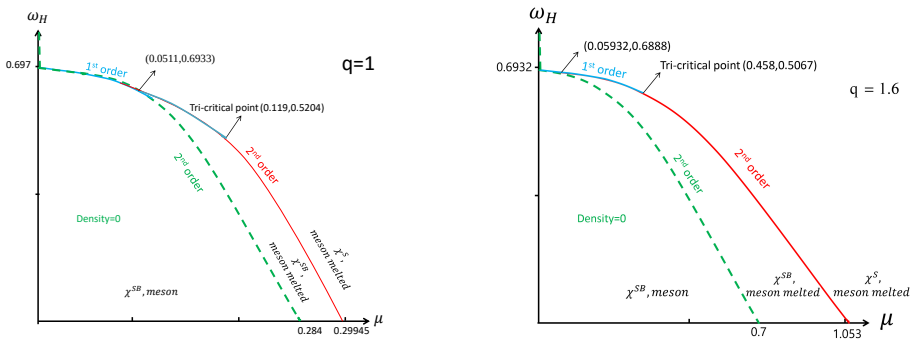

Figure 5: Effect of chiral symmetry breaking parameter q on the phase diagram of the QCD-like theory.

statistical ensembles can indeed yield different insights into the behavior of a system. In the canonical ensemble, the number of particles, volume, and temperature are fixed, leading to a specific set of microstates for the system. The grand canonical ensemble, on the other hand, allows for the exchange of both energy and particles with a reservoir, which means that the chemical potential, volume, and temperature are the fixed parameters. When considering a phase diagram with zero quark mass, it's important to note that the mass of quarks significantly impacts the properties of the QCD phase transition. At zero baryon density, the phase diagram can change qualitatively when quark masses are taken to be zero. This is often represented in the Columbia plot, which summarizes the qualitative features of the QCD phase transition and shows how the order of the phase transition changes with the quark masses [32]. In the context of the grand canonical ensemble, the phase diagram

with zero quark mass would reflect the behavior of the system in terms of temperature and chemical potential without the influence of quark mass, which is an important consideration in the study of chiral symmetry and its restoration at high temperatures or densities. The absence of quark mass leads to a simplification of the QCD phase diagram and can reveal fundamental aspects of the theory, such as the nature of the chiral phase transition.

The meson melting transition at finite density is second order in QCD. A second-order phase transition is characterized by a continuous change in the order parameter and no latent heat. In the context of QCD, this means that as the system crosses the transition point, properties such as the quark-antiquark condensate change smoothly, and there is no sudden release or absorption of energy. At finite density, the reason meson melting is second order can be attributed to the gradual dissolution of mesons into their constituent quarks due to the increasing density and interactions with the thermal medium. As the baryon density increases, the conditions become unfavorable for the binding of quarks into mesons, leading to their melting. This process does not happen abruptly but rather progressively as the density reaches a critical point. The meson melting transition is also influenced by the behavior of the chiral condensate. At low densities, the chiral condensate provides mass to the quarks through spontaneous chiral symmetry breaking. However, as the density increases, the condensate diminishes, leading to the restoration of chiral symmetry and the melting of mesons.

In our massless theoretical framework, we have observed a direct phase shift of the first order. This shift moves from a phase where chiral symmetry is broken and mesons are stable bound states, to a phase where chiral symmetry is intact and mesons have disintegrated. Along the axis of finite density, the transition of meson disintegration is of the second order and is distinct from another second-order transition that reinstates chiral symmetry. It is evident that the temperature-chemical potential phase diagram must contain at least one critical endpoint. The phase diagram for our massless model is presented in Figure 5.

There are two plots in this figure for different values of q. In this figure, the dashed green line represents the condition where the density is zero, marking the second-order meson melting transition. This transition signifies a shift from a Minkowski embedding to a black hole embedding. During this transition, the density starts at zero and increases continuously. Simultaneously, the quark condensate begins to decrease smoothly from its fixed value in the Minkowski phase. The quark condensate's behavior remains continuous throughout this transition. It's important to note that while the slope of the embedding at the UV boundary remains continuous across the transition, the embedding in the IR low energy is discontinuous, indicating a change in the topology of the D7-brane embeddings.

The blue line signifies a first-order transition, characterized by abrupt changes in properties such as density and the chiral condensate. On the other hand, the red dotted line indicates a second-order transition where these changes occur smoothly. The red dotted line is particularly noteworthy because it represents a phase boundary that is only present when the quark mass is zero. This is due to the fact that this boundary is associated with the spontaneous breaking of chiral symmetry, a phenomenon that occurs exclusively in the massless limit of quarks. In essence, the massless condition is crucial for the existence of this phase boundary, as it is intimately linked to the fundamental symmetries of the QCD phase diagram.

The diagram clearly marks two tri-critical points, which are pivotal in understanding the phase transitions within the system. Identifying these points numerically is a direct process. The junction of the first and second order chiral symmetry restoration transitions is located at the coordinates $(\mu, w_H) = (0.0511, 0.6933)$. Meanwhile, the second tri-critical point, where the meson melting transitions converge, is found at $(\mu, w_H) = (0.119, 0.5204)$. These critical points are essential for delineating the boundaries between different phases and

for predicting the behavior of the system under varying conditions of temperature, density, and magnetic field. While the study presented results for the grand canonical ensemble, it suggests that the phase diagram can also be examined in the canonical ensemble.

In summary, we have examined the impact of chiral symmetry breaking on the critical point in QCD-like theories. These theories, while sharing similarities with QCD, may differ in the number of colors, flavors, or additional symmetries. They play a crucial role in investigating various aspects of strong interactions and the complex phenomena within QCD, especially in the non-perturbative regime. The phase diagram of these theories is an invaluable tool for exploring phase transitions and understanding the properties of the QGP. In this paper, we employed holography and utilized an adapted D3/D7 framework. This is because the original D3/D7 model provides a simplistic representation of the massive, deconfined quark phase with chiral symmetry breaking. The adapted model suggests the possibility of creating a more accurate model that includes explicit chiral symmetry breaking, which could enhance our understanding of the phase diagram. We introduced a new dilaton profile to control the anomalous condensate of quark-antiquark pairs with parameter q and demonstrated how this profile affects chiral symmetry breaking, a pivotal phenomenon in understanding the behavior of strong interactions. The final results, depicted in Figure 5, show that the critical endpoint moves towards regions of higher temperature and lower potential as the q parameter increases.

Acknowledgment

We would like to thank Nick Evans and Matthew Russell for their collaboration on this project in the early stages.

Authors' Contributions

All authors have the same contribution.

Data Availability

The manuscript has no associated data or the data will not be deposited.

Conflicts of Interest

The authors declare that there is no conflict of interest.

Ethical Considerations

The authors have diligently addressed ethical concerns, such as informed consent, plagiarism, data fabrication, misconduct, falsification, double publication, redundancy, submission, and other related matters.

Funding

This research did not receive any grant from funding agencies in the public, commercial, or non-profit sectors.

References

[1] M. A. Stephanov, "QCD phase diagram: An Overview", PoS **LAT2006**, 024 (2006). DOI: 10.22323/1.032.0024 [arXiv:hep-lat/0701002 [hep-lat]]

[2] Y. Hatta and T. Ikeda, "Universality, the QCD critical / tricritical point and the quark number susceptibility", Phys. Rev. D **67**, 014028 (2003). DOI: 10.1103/PhysRevD.67.014028 [arXiv:hep-ph/0210284 [hep-ph]]

[3] K. Fukushima and T. Hatsuda, "The phase diagram of dense QCD", Rept. Prog. Phys. **74**, 014001 (2011). DOI: 10.1088/0034-4885/74/1/014001 [arXiv:1005.4814 [hep-ph]]

[4] E. Laermann and O. Philipsen, "The Status of lattice QCD at finite temperature", Ann. Rev. Nucl. Part. Sci. **53**, 163 (2003). DOI: 10.1146/annurev.nucl.53.041002.110609 [arXiv:hep-ph/0303042 [hep-ph]]

[5] A. Barducci, R. Casalbuoni, S. De Curtis, R. Gatto, and G. Pettini, "Chiral Phase Transitions in QCD for Finite Temperature and Density", Phys. Rev. D **41**, 1610 (1990). DOI: 10.1103/PhysRevD.41.1610

[6] C. D. Roberts and S. M. Schmidt, "Dyson-Schwinger equations: Density, temperature and continuum strong QCD", Prog. Part. Nucl. Phys. **45**, S1 (2000). DOI: 10.1016/S0146-6410(00)90011-5 [arXiv:nucl-th/0005064 [nucl-th]]

[7] J. M. Maldacena, "The Large N limit of superconformal field theories and supergravity", Adv. Theor. Math. Phys. **2**, 231 (1998). DOI: 10.1023/A:1026654312961 [arXiv:hep-th/9711200 [hep-th]]

[8] S. S. Gubser, I. R. Klebanov, and A. M. Polyakov, "Gauge theory correlators from noncritical string theory", Phys. Lett. B **428**, 105 (1998). DOI: 10.1016/S0370-2693(98)00377-3 [arXiv:hep-th/9802109 [hep-th]]

[9] E. Witten, "Anti-de Sitter space and holography", Adv. Theor. Math. Phys. **2**, 253 (1998). DOI: 10.4310/ATMP.1998.v2.n2.a2 [arXiv:hep-th/9802150 [hep-th]]

[10] M. Grana and J. Polchinski, "Gauge-gravity duals with holomorphic dilaton", Phys. Rev. **D65**, 126005 (2002). [arXiv:hep-th/0106014]

[11] A. Karch and E. Katz, "Adding flavor to AdS/CFT", JHEP **0206**, 043 (2002). [arXiv:hep-th/0205236]

[12] M. Kruczenski, D. Mateos, R. C. Myers, and D. J. Winters, "Meson spectroscopy in AdS-CFT with flavor", JHEP **0307**, 049 (2003). [arXiv:hep-th/0304032]

[13] J. Erdmenger, N. Evans, I. Kirsch, and E. Threlfall, "Mesons in Gauge/Gravity Duals-A Review", Eur. Phys. J. A **35**, 81 (2008). [arXiv:0711.4467 [hep-th]]

[14] N. Evans, A. Gebauer, K. Y. Kim, and M. Magou, "Holographic Description of the Phase Diagram of a Chiral Symmetry Breaking Gauge Theory", JHEP **03**, 132 (2010). DOI: 10.1007/JHEP03(2010)132 [arXiv:1002.1885 [hep-th]]

[15] A. Belyaev, K. Bitaghsir Fadafan, N. Evans, and M. Gholamzadeh, "Any room left for technicolor? Holographic studies of NJL assisted technicolor", Phys. Rev. D **101**, 086013 (2020). DOI: 10.1103/PhysRevD.101.086013 [arXiv:1910.10928 [hep-ph]]

[16] K. Bitaghsir Fadafan, J. Cruz Rojas, and N. Evans, "Deconfined, Massive Quark Phase at High Density and Compact Stars: A Holographic Study", Phys. Rev. D **101**, 126005 (2020). DOI: 10.1103/PhysRevD.101.126005 [arXiv:1911.12705 [hep-ph]]

[17] C. Hoyos, D. Rodríguez Fernández, N. Jokela, and A. Vuorinen, "Holographic quark matter and neutron stars", Phys. Rev. Lett. **117**, 032501 (2016). DOI: 10.1103/PhysRevLett.117.032501 [arXiv:1603.02943 [hep-ph]]

[18] R. Alvares, N. Evans, and K. Y. Kim, "Holography of the Conformal Window", Phys. Rev. D **86**, 026008 (2012). DOI: 10.1103/PhysRevD.86.026008 [arXiv:1204.2474 [hep-ph]]

[19] M. Atashi and K. B. Fadafan, "Anomalous dimension and quasinormal modes of flavor branes", [arXiv:2203.10468 [hep-th]]

[20] V. G. Filev, C. V. Johnson, R. C. Rashkov, and K. S. Viswanathan, "Flavoured large N gauge theory in an external magnetic field", JHEP **10**, 019 (2007). DOI: 10.1088/1126-6708/2007/10/019 [arXiv:hep-th/0701001 [hep-th]]

[21] K. Peeters, J. Sonnenschein, and M. Zamaklar, "Holographic melting and related properties of mesons in a quark gluon plasma", Phys. Rev. D **74**, 106008 (2006). [arXiv:hep-th/0606195]

[22] C. Hoyos-Badajoz, K. Landsteiner, and S. Montero, "Holographic Meson Melting", JHEP **0704**, 031 (2007). [arXiv:hep-th/0612169]

[23] J. Babington, J. Erdmenger, N. J. Evans, Z. Guralnik, and I. Kirsch, "Chiral symmetry breaking and pions in non-supersymmetric gauge / gravity duals", Phys. Rev. D **69**, 066007 (2004). [arXiv:hep-th/0306018]

[24] R. Apreda, J. Erdmenger, N. Evans, and Z. Guralnik, "Strong coupling effective Higgs potential and a first order thermal phase transition from AdS/CFT duality", Phys. Rev. D **71**, 126002 (2005). [arXiv:hep-th/0504151]

[25] T. Albash, V. G. Filev, C. V. Johnson, and A. Kundu, "A topology-changing phase transition and the dynamics of flavour", Phys. Rev. D **77**, 066004 (2008). [arXiv:hep-th/0605088]

[26] D. Mateos, R. C. Myers, and R. M. Thomson, "Holographic phase transitions with fundamental matter", Phys. Rev. Lett. **97**, 091601 (2006). [arXiv:hep-th/0605046]

[27] D. Mateos, R. C. Myers, and R. M. Thomson, "Thermodynamics of the brane", JHEP **0705**, 067 (2007). [arXiv:hep-th/0701132]

[28] X. Chen and M. Huang, "Flavor dependent Critical endpoint from holographic QCD through machine learning", [arXiv:2405.06179 [hep-ph]]

[29] M. Matsumoto, "Tricritical phenomena in holographic chiral phase transitions", JHEP **11**, 107 (2022). DOI: 10.1007/JHEP11(2022)107 [arXiv:2208.02605 [hep-th]]

[30] D. Endo, Y. Fukazawa, M. Matsumoto, and S. Nakamura, "Electric-field driven nonequilibrium phase transitions in AdS/CFT", JHEP **03**, 173 (2023). DOI: 10.1007/JHEP03(2023)173 [arXiv:2302.13535 [hep-th]]

[31] A. Karch and A. O'Bannon, "Holographic Thermodynamics at Finite Baryon Density: Some Exact Results", JHEP **0711**, 074 (2007). [arXiv:0709.0570 [hep-th]]

[32] K. Chelabi, Z. Fang, M. Huang, D. Li, and Y. L. Wu, "Chiral Phase Transition in the Soft-Wall Model of AdS/QCD", JHEP **04**, 036 (2016). DOI: 10.1007/JHEP04(2016)036 [arXiv:1512.06493 [hep-ph]]